Detection of structural asymmetries in Forksheet FET arrays using Mueller matrix ellipsometry: a theoretical study

Boglárka Dikó, Roberta Zsófia Kiss, Dávid Egri, and Emeric Balogh*

Semilab Semiconductor Physics Laboratory Co. Ltd., Budapest, Hungary

ABSTRACT. **Background:** With the appearance of ever-smaller transistors and new structures, new metrological challenges also arise, including the detection of different structural defects. Mueller matrix (MM) measurement can provide an opportunity to investigate them.

Aim: Defects can cause a deterioration in device performance; therefore, their characterization is particularly important. Our goal is to investigate the possibility of detecting asymmetry defects using MM measurement and to study the distinguishability of these structural imperfections in the case of forksheet field-effect transistor (FET).

Approach: Simulation of MM measurements with different degrees and directions of forksheet FET's profile asymmetries. To quantify the distinguishability of the optical responses caused by the defects, the correlation between the asymmetry parameters was calculated. Since the precise alignment of a sample is a key factor in the detection of asymmetries, the effect of the alignment uncertainty and a method for filtering it out were also investigated.

Results and Conclusions: MM measurement is sensitive to both the magnitude and direction of the profile bending and the shift of the dielectric wall. The correlation coefficients show that the optical responses of the asymmetry defects and the alignment error can be distinguished. The latter can even be eliminated with a method presented in this article.

1 Introduction

In the world of complementary metal-oxide semiconductor (CMOS) technology, there are ever-increasing demands for more efficient and faster devices, which include the development of ever smaller and more complex transistors.

A step forward in shrinking the size of the transistors is projected to be the appearance of forksheet field-effect transistor (FET) based devices. This is an evolution of the nanosheet architecture, where a dielectric wall is added between the n-channel metal-oxide semiconductor (NMOS) and p-channel metal-oxide semiconductor (PMOS) devices, allowing a tighter arrangement. Based on simulations this is projected to enable a performance increase of up to 10%, a 24% energy efficiency improvement and reduced cell area by 20% compared to a nanosheet

---

*Address all correspondence to Emeric Balogh, emeric.balogh@semilab.hu

FET.[1] However, the dimension of the defects that may occur in the structures does not change, so their effect becomes increasingly significant.[2] The non-uniformities can reduce the performance of the device; the leakage current may increase, and it also affects the CMOS threshold voltage.[2,3]

For these transistors to work as efficiently as possible, it is particularly important to monitor the complex, multi-step processes, and reveal the possible imperfections. With the appearance of new devices, new types of defects also arise, which require new metrological solutions. The modified process steps used in the case of front end of line (FEOL) forksheet FET manufacturing, may result in new types of defects instead of or in addition to the typical ones present in previous structures (e.g., pitch-walking, overlay-error, fin-bending, line width roughness, line edge roughness, etc.[2,4]). During the lithography process, the structure may bend or/and the length of the nanosheets may differ on opposite sides of the wall.

The ideal solution to detect the imperfections is a fast, non-destructive, non-contact, metrology, which allows in-line measurement of the samples, such as optical critical dimension (OCD) metrology. This technique includes spectroscopic reflectometry (SR), conventional spectroscopic ellipsometry (SE), and Mueller matrix spectroscopic ellipsometry (MM-SE) as well. These are mostly model-based methods where a theoretical model is built to calculate the light–matter interaction of the specific structure and obtain the reflectance or transmittance spectra using the rigorous coupled wave analysis (RCWA) method. The spectra depend on the parameters of the structure, and regression-based fitting can be used to determine the parameters of interest.[5] Among these, the MM-SE measurement is the most complete, and as such, it promises to be the most suitable to measure structural defects and especially structural asymmetries. This is, because it fully describes the changes in the polarized state of light upon interaction with the sample—not only the cross-polarization but also depolarization can be detected with its help.[6]

In this paper, we analyze the possibilities of using MM–based analysis to detect structural asymmetry defects arising during the forksheet FET fabrication process. We calculate measurement sensitivity and correlations for the MM-SE method to selected asymmetric features and highlight the advantages of using the method in detecting these defects. The possibilities of detecting and eliminating alignment errors that may arise during the measurement were also investigated. The simulations are all based on the prototype forksheet FET structure parameters fabricated by imec during the development of 2 nm technology node. We used R-Soft commercial software to calculate the theoretical MM response of the structure.

2 Methods

2.1 Sample

The investigated structure was based on the sample provided to Semilab Ltd. within the framework of the IT2 (Integrated Circuit Technology for the 2 nm node) project. The sample was manufactured by imec, and it is based on the most advanced, 2 nm technology nodes. The analyzed structure arises during the FEOL process, before the forksheet release process step, i.e., when the SiGe sacrificial layer will be completely etched between the Si sheets to reveal the nanosheets, which will become the channels of the MOS devices. This is a so-called short loop sample, in which the gate was not formed, therefore it has a two-dimensional geometry.[7,8] Transmission electron microscopy (TEM) images of the structure were used to build and parameterize the theoretical model in R-Soft (Fig. 1).

2.2 Simulation Method

During an OCD type measurement using MM-SE, the change in the state of polarization of the incidence linearly polarized light is measured upon reflection from a grating like structure. Let us denote the amplitudes of s and p polarization light waves incident on a sample as E_s^i and E_p^i, respectively. In the same manner, we define the reflected light amplitudes E_s^r and E_p^r in the case of the zeroth diffraction order (Fig. 2).

To simulate such an optical response of the structures of interest the RCWA method was utilized. For this purpose, the RSoft Photonic Device Tools made by Synopsys was used where the DiffractMOD simulation tool was chosen for this study.
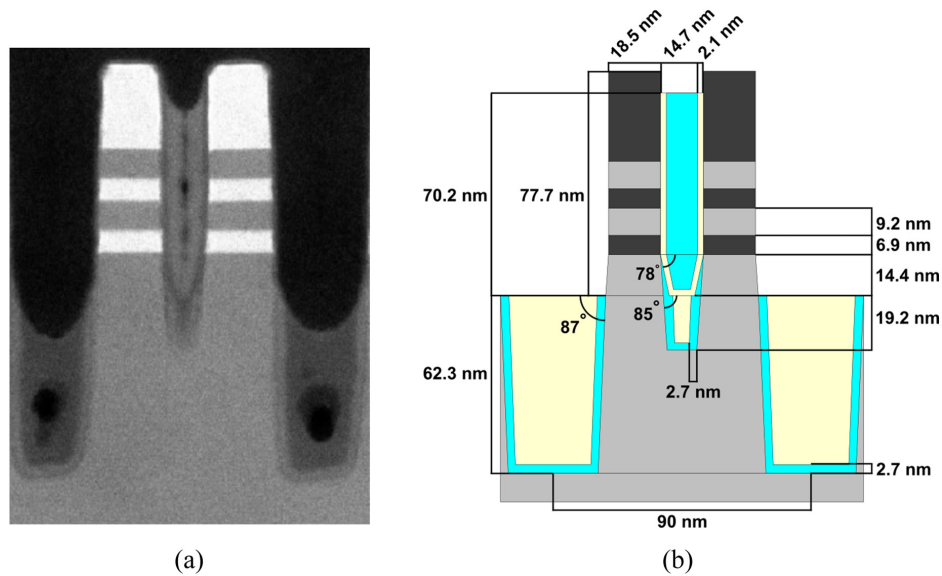
Fig. 1 (a) TEM image of the sample and (b) the structure built in RSoft. Black color represents $Si_{0.75}Ge_{0.25}$, gray Si, green Si_3N_4, and yellow SiO_2 (the semicircular cavities that can be seen on the TEM image are TEM imaging artifacts).
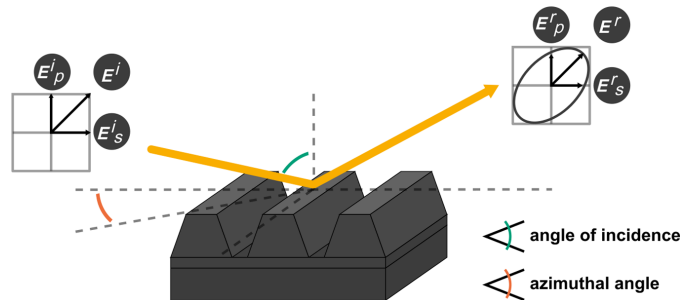
Fig. 2 The change in the state of polarization of the incident light upon reflection from the grating like structure. It also illustrates the angle of incidence and the azimuthal angle.

The RCWA method is an industry standard in case of OCD measurements because of the beneficial properties, such as speed, accuracy, and robustness, of the solution for diffraction type problems in case of subwavelength grating-like structures. It was first introduced by Moharam and Gaylord in the 1980s and improved over time.[9–12] The method takes advantage of the periodic nature of the structure with solving the Maxwell equations in Fourier space. The solution comes in a Fourier series form where the different Fourier components can be associated with diffraction orders.[13] To apply this simulation technique to complex structures, such as ones with bended sidewalls, the structure must be broken down into binary layers. In this case, the equations are solved for every layer and the solution is combined to calculate the full optical response of the grating.[12] With these two main concepts numerical approximation must be made regarding the number Fourier modes and the number of binary layers used. These numerical parameters must be chosen carefully to provide a physically correct solution while also producing a reasonable computational time.

In this study, MM-SE was investigated where the optical response of the structures of interest must be modeled in the form of MMs. In case of non-depolarizing samples, the change in the polarization state can be described in the context of the Jones formalism [Eq. (1)].[14] The polarization state is described by the Jones vectors consisting of the complex amplitude of the s- and p-polarization components of the light. The reflection from the sample is described by the Jones matrix consisting of the complex reflection coefficients:

$$\begin{bmatrix} E_p^r \\ E_s^r \end{bmatrix} = \begin{bmatrix} r_{pp} & r_{ps} \\ r_{sp} & r_{ss} \end{bmatrix} \begin{bmatrix} E_p^i \\ E_s^i \end{bmatrix}. \tag{1}$$

In case of a general anisotropic sample, the r_{ps} and r_{sp} cross-terms describe the anisotropic characteristics where the sample rotates the incident polarization, generating reflected p polarized light from the incident s-polarized waves, and the other way around as well. Grating-like structures can be described as anisotropic samples because they show different optical properties parallel and perpendicular to the grating lines. This is often called geometrical anisotropy because it is linked to geometric properties of the structure.

In case of no depolarization, the MM of the sample can be calculated within the Jones–Mueller formalism [Eq. (2)] where the Re and Im notations represent the real and imaginary parts of the enclosed complex quantities.[14] In the practice of MM spectral ellipsometry, the normalized version of the MM by the MM_{11} element is measured and analyzed:

$MM=$

$$\begin{bmatrix} \frac{1}{2}(|r_{pp}|^2+|r_{sp}|^2+|r_{ps}|^2+|r_{ss}|^2) & \frac{1}{2}(|r_{pp}|^2+|r_{sp}|^2-|r_{ps}|^2-|r_{ss}|^2) & \mathrm{Re}(r_{pp}r_{ps}^*+r_{sp}r_{ss}^*) & \mathrm{Im}(r_{pp}r_{ps}^*+r_{sp}r_{ss}^*) \\ \frac{1}{2}(|r_{pp}|^2-|r_{sp}|^2+|r_{ps}|^2-|r_{ss}|^2) & \frac{1}{2}(|r_{pp}|^2-|r_{sp}|^2-|r_{ps}|^2+|r_{ss}|^2) & \mathrm{Re}(r_{pp}r_{ps}^*-r_{sp}r_{ss}^*) & \mathrm{Im}(r_{pp}r_{ps}^*-r_{sp}r_{ss}^*) \\ \mathrm{Re}(r_{pp}r_{sp}^*+r_{ps}r_{ss}^*) & \mathrm{Re}(r_{pp}r_{sp}^*-r_{ps}r_{ss}^*) & \mathrm{Re}(r_{pp}r_{ss}^*+r_{ps}r_{sp}^*) & \mathrm{Im}(r_{pp}r_{ss}^*-r_{ps}r_{sp}^*) \\ -\mathrm{Im}(r_{pp}r_{sp}^*+r_{ps}r_{ss}^*) & -\mathrm{Im}(r_{pp}r_{sp}^*-r_{ps}r_{ss}^*) & -\mathrm{Im}(r_{pp}r_{ss}^*+r_{ps}r_{sp}^*) & \mathrm{Re}(r_{pp}r_{ss}^*-r_{ps}r_{sp}^*) \end{bmatrix} \tag{2}$$

3 Symmetry Relations to Consider in Mueller Matrix Measurements

In the following theoretical discussion, we assume that all the constituting materials of the grating structure are optically isotropic, nonmagnetic, not optically active, and the sample does not depolarize the beam.

In the case of reflection from diffraction gratings periodic along one direction, there are two special measurement configurations regarding the azimuthal angle: $\varphi = 0$ deg and $\varphi = 90$ deg. The case of $\varphi = 0$ deg is called planar incidence, because all diffracted orders remain in the plane of incidence. In this case, cross-polarization terms vanish ($r_{sp} = r_{ps} = 0$), the off-diagonal blocks in the MM become zero.

The case of $\varphi = 90$ deg is a special case of conical diffraction (diffracted orders lie on a cone). In this case, cross-polarization terms vanish only if the grating structure has reflection symmetry to the plane of incidence ($r_{sp} = r_{ps} = 0$).[15]

Occurrence of cross-polarization ($r_{sp} \neq 0$, $r_{ps} \neq 0$, resulting in nonzero off-diagonal block elements of MM) is observed: (1) at any azimuthal angle other than 0 deg or 90 deg, or (2) in the absence of reflection symmetry in $\varphi = 90$ deg measurement configuration.

Using the reciprocity theorem by Vincent and Nevière—derived from the Lorentz reciprocity theorem—symmetry relations of the MM can be deduced for special cases.[5,15–17] According to this, in case of symmetric structures, the sample Jones matrix is antisymmetric ($r_{sp} = -r_{ps}$). Rewriting the MM, we get symmetry properties between the top and bottom triangles as shown in Eq. (3). This relation has been used to identify structural asymmetry in measurements performed at arbitrary azimuthal angles:[18]

$$MM = \begin{bmatrix} MM_{11} & MM_{12} & MM_{13} & MM_{14} \\ MM_{12} & MM_{22} & MM_{23} & MM_{24} \\ -MM_{13} & -MM_{23} & MM_{33} & MM_{34} \\ MM_{14} & MM_{24} & -MM_{34} & MM_{44} \end{bmatrix}. \tag{3}$$

From the reciprocity theorem, it also shows that in the case of symmetric grating profiles, when the grating is measured at the opposite azimuthal angle $(-\varphi, +\varphi)$, the off-diagonal

elements have opposite signs, but their absolute values remain the same. It also holds true that if the grating is rotated by 180 deg, none of the elements of the MM will change.[19]

In another special case, when the measurement is performed at exactly $\varphi = 90$ deg azimuthal angle and the structure is asymmetric, the following relation holds: $r_{sp} = r_{ps}$[15,20] In this case, the symmetry properties of the MM are as in Eq. (4):

$$MM = \begin{bmatrix} MM_{11} & MM_{12} & MM_{13} & MM_{14} \\ MM_{12} & MM_{22} & MM_{23} & MM_{24} \\ MM_{13} & MM_{23} & MM_{33} & MM_{34} \\ -MM_{14} & -MM_{24} & -MM_{34} & MM_{44} \end{bmatrix}. \tag{4}$$

These symmetry relations can also be used to identify if the source of non-zero off-diagonal MM elements in measurements arise from structural asymmetry or from an inaccurately aligned sample.

The off-diagonal elements are sensitive not only to the asymmetry but also to its direction.[19,21–24] If a measurement is performed at $\varphi = 90$ deg and then the grating is rotated by 180 deg (measuring at $\varphi = -90$ deg), the off-diagonal elements change sign. This is equivalent to measuring a structure that is asymmetric in the opposite direction (i.e., mirrored to the plane of incidence) at the same azimuthal angle.

At arbitrary azimuthal angles, for asymmetric structures, such general MM symmetry relations as shown in Eqs. (3) and (4) were not identified. The $\varphi = 90$ deg configuration is thus the most advantageous to detect structural asymmetry defects, because only the source of non-zero off-diagonal elements is the profile asymmetry. This has been verified and shown that in any other measurement configuration the different sources of the non-zero off-diagonal elements mix, making it more difficult to identify the profile asymmetry, and the sensitivity may disappear at azimuth 0 deg.[19–23]

As a consequence, special attention is required for the precise alignment of the sample before measurement, as any deviation from $\varphi = 90$ deg leads to off-diagonal responses itself, which can be misleading. Using an ellipsometry tool with a precise rotation stage, the following test can be performed to identify the source of the MM off-diagonal response. If the measurement is performed close to an azimuthal angle of 90 deg, and then another after rotating the sample by 180 deg, the alignment error can be distinguished from the asymmetry effects by subtracting the two spectra from each other due to the following relation:[19] in a general case $r_{ps}^{x^\circ} = -r_{sp}^{x+180^\circ}$ (where x represents an arbitrary azimuthal angle), then the MM of the rotated measurement can be written with the elements of the initial one Eq. (5):

$$MM^{x+180^\circ} = \begin{bmatrix} MM_{11}^{x^\circ} & MM_{21}^{x^\circ} & -MM_{31}^{x^\circ} & MM_{41}^{x^\circ} \\ MM_{12}^{x^\circ} & MM_{22}^{x^\circ} & -MM_{32}^{x^\circ} & MM_{42}^{x^\circ} \\ -MM_{13}^{x^\circ} & -MM_{23}^{x^\circ} & MM_{33}^{x^\circ} & -MM_{43}^{x^\circ} \\ MM_{14}^{x^\circ} & MM_{24}^{x^\circ} & -MM_{34}^{x^\circ} & MM_{44}^{x^\circ} \end{bmatrix}. \tag{5}$$

If we subtract MM^{x° from MM^{x+180° and rewrite the difference matrix with the Jones matrix elements, we get

$$
\mathrm{MM}^{x^\circ} - \mathrm{MM}^{x+180^\circ} =
\begin{bmatrix}
0 & |r_{\mathrm{sp}}|^2 - |r_{\mathrm{ps}}|^2 & \mathrm{Re}(r_{\mathrm{pp}}(r^*_{\mathrm{ps}} + r^*_{\mathrm{sp}}) + (r_{\mathrm{sp}} + r_{\mathrm{ps}})r^*_{\mathrm{ss}}) & \mathrm{Im}(r_{\mathrm{pp}}(r^*_{\mathrm{ps}} + r^*_{\mathrm{sp}}) + (r_{\mathrm{sp}} + r_{\mathrm{ps}})r^*_{\mathrm{ss}}) \\
|r_{\mathrm{sp}}|^2 - |r_{\mathrm{ps}}|^2 & 0 & \mathrm{Re}(r_{\mathrm{pp}}(r^*_{\mathrm{ps}} + r^*_{\mathrm{sp}}) - (r_{\mathrm{sp}} + r_{\mathrm{ps}})r^*_{\mathrm{ss}}) & \mathrm{Im}(r_{\mathrm{pp}}(r^*_{\mathrm{ps}} + r^*_{\mathrm{sp}}) - (r_{\mathrm{sp}} + r_{\mathrm{ps}})r^*_{\mathrm{ss}}) \\
\mathrm{Re}(r_{\mathrm{pp}}(r^*_{\mathrm{ps}} + r^*_{\mathrm{sp}}) + (r_{\mathrm{sp}} + r_{\mathrm{ps}})r^*_{\mathrm{ss}}) & \mathrm{Re}(r_{\mathrm{pp}}(r^*_{\mathrm{ps}} + r^*_{\mathrm{sp}}) - (r_{\mathrm{sp}} + r_{\mathrm{ps}})r^*_{\mathrm{ss}}) & 0 & -2\mathrm{Im}(r_{\mathrm{ps}} r^*_{\mathrm{sp}}) \\
-\mathrm{Im}(r_{\mathrm{pp}}(r^*_{\mathrm{ps}} + r^*_{\mathrm{sp}}) + (r_{\mathrm{sp}} + r_{\mathrm{ps}})r^*_{\mathrm{ss}}) & -\mathrm{Im}(r_{\mathrm{pp}}(r^*_{\mathrm{ps}} + r^*_{\mathrm{sp}}) - (r_{\mathrm{sp}} + r_{\mathrm{ps}})r^*_{\mathrm{ss}}) & -2\,\mathrm{Im}(r_{\mathrm{ps}} r^*_{\mathrm{sp}}) & 0
\end{bmatrix}
\tag{6}
$$

Investigating a grating with symmetric profile, MM^{x° and $\mathrm{MM}^{x+180^\circ}$ are equivalent because of the symmetries of the MM, so all the elements of the matrix in Eq. (6) will be zero. This will not be true for asymmetric gratings. However, if the measurement is performed at ±90, 0 deg azimuthal angle and the grating profile is asymmetric, then $r_{sp} = r_{ps}$, resulting in nonzero off-diagonal and zero on-diagonal elements. If the azimuthal angle deviates from ±90 deg with a small ϵ angle, then $r_{sp} \simeq r_{ps} \simeq (r_{sp} + r_{ps})/2$, therefore the off-diagonal blocks of the MM ($\mathrm{MM}_{\mathrm{off}}$) can be approximated as

$$
\mathrm{MM}^{90^\circ}_{\mathrm{off}} \simeq (\mathrm{MM}^{90^\circ - \epsilon}_{\mathrm{off}} - \mathrm{MM}^{-90^\circ - \epsilon}_{\mathrm{off}})/2.
\tag{7}
$$

With this method, one can filter out the effect of the alignment error, and the effect of the asymmetry can be isolated.

4 Simulation Results

The following structural asymmetry features were analyzed:

- the bending of the entire structure [Fig. 3(a)], in the following we will refer to this as fin bending angle (FBA).
- left-right asymmetry, resulting from the shift of the central dielectric wall separating the NMOS and PMOS devices [Fig. 3(b)]. Referred to as central wall shift (CW shift).

Because, in practice, the alignment of the sample may not always be completely accurate, which could lead to misleading conclusions, the effect of alignment accuracy on the measurements was also studied through simulations. This is used to determine whether these different effects (asymmetries and alignment error)—that could all cause an off-diagonal response in an MM measurement—could be distinguished from each other.
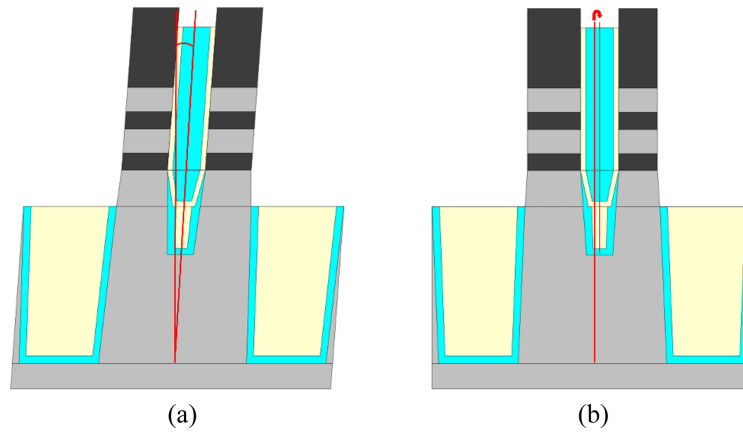
Fig. 3 Illustration of the investigated asymmetrical features. (a) FBA and (b) CW shift.

4.1 Sensitivity Analysis for Changes in FBA, CW Shift, and Azimuthal Angle around 90 deg

Since the off-diagonal elements of the MM are most sensitive to the asymmetries at 90 deg azimuthal angle, the simulations were performed for this scenario. An angle of incidence of 70 deg, in the spectral range of 193 to 900 nm was modeled, a common configuration in spectral ellipsometry. During the simulations, the literature values of the refractive index and extinction coefficient of the materials were used.

To investigate the effect of different parameters, simulations were run with a number of asymmetry defects included in the model (Table 1). The MM spectra obtained for different FBA and CW shift values are shown in Figs. 4 and 5, respectively. The effect of a slight deviation from 90 deg azimuthal angle on the MM was also investigated (Fig. 6). During the simulation of the optical response of MM for a given parameter change, the values of the other parameters were at the nominal level.

Since the upper 2×2 off-diagonal elements (MM_{13}, MM_{14}, MM_{23}, MM_{24}) have the same absolute values as the lower 2×2 elements (MM_{31}, MM_{32}, MM_{41}, MM_{42}) [Eq. (4)], the following conclusions will be drawn only on the upper elements.

According to the simulations, the off-diagonal elements are sensitive to both the magnitude and direction of present asymmetry and alignment error. The on-diagonal elements provide very subtle response to the asymmetry and are not sensitive to its direction at all.

In case of bending, the MM_{23} element shows the highest sensitivity (Fig. 4). For the presence of CW shift, in the UV range MM_{24} provides the largest optical response (around 200 nm), while in the visible range MM_{14}, MM_{23}, and MM_{24} give responses of similar magnitude (Fig. 5). However, the magnitudes of the effects caused by CW shift and FBA are quite small, which can be overshadowed by the measurement noise. The measurement accuracy must be in the order of 0.02 to detect 1 deg FBA or 0.01 to perceive 1 nm CW shift. If the sample is not aligned exactly at 90 deg azimuthal angle, MM_{13} will be the most sensitive to this error, but the other elements also give a significant response (Fig. 6) in this case.

Table 1 Parameter values investigated during the simulations.

Parameter	Nominal value	Step	Range
FBA (deg)	0	1	−2 to 2
CW shift (nm)	0	1	−2 to 2
φ (deg)	90	1	88 to 92
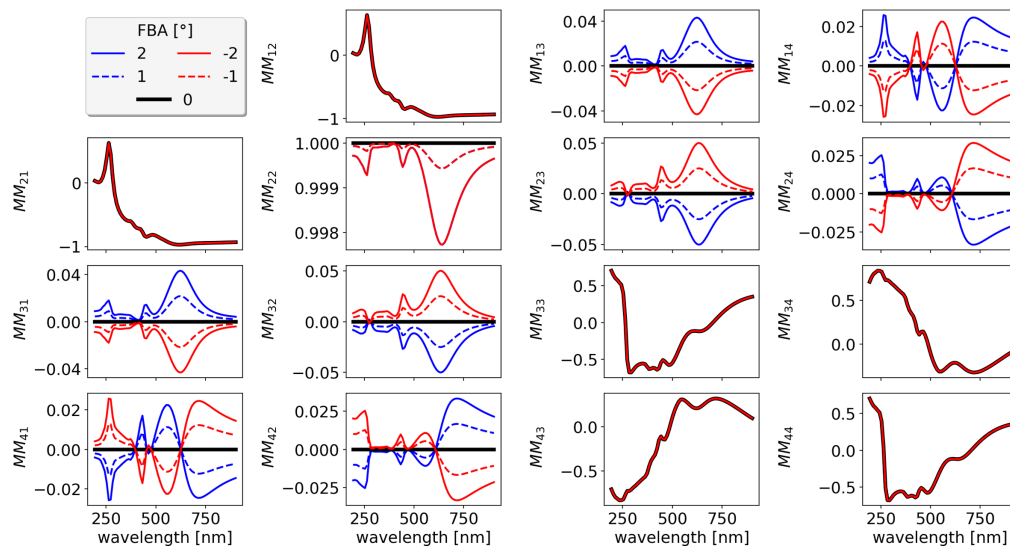
Fig. 4 MM for different FBA values. The off-diagonal elements provide a significant response to the direction and degree of profile bending, with element MM_{23} showing the highest sensitivity.
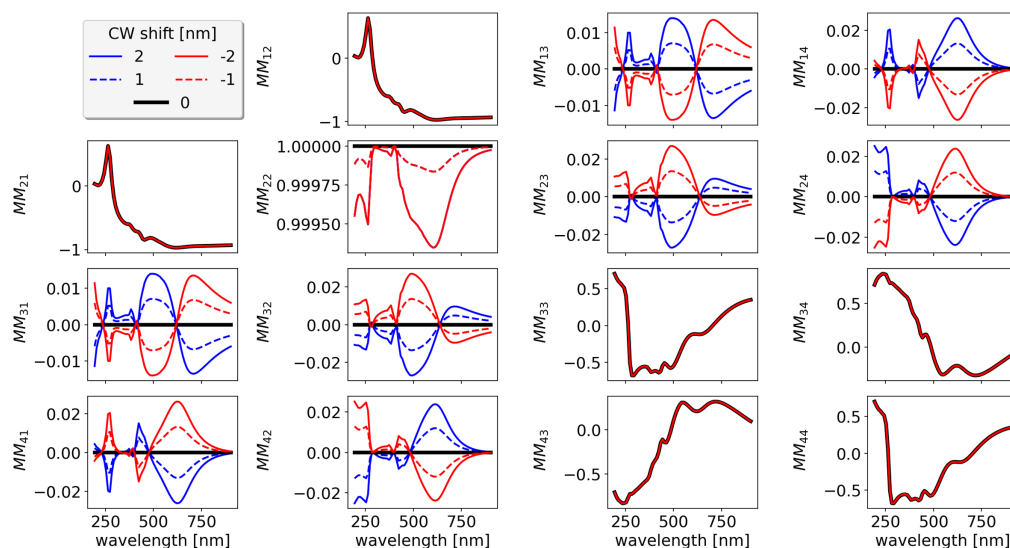
Fig. 5 MM for different CW shift values. The shift of the central wall is clearly noticeable on the off-diagonal elements.

4.2 Investigating Correlations Between the Asymmetry Parameters

The correlation between the different parameters was also investigated to quantify the distinguishability of their effects. The correlation matrix was calculated based on the method discussed by Vagos et al.[25] If there is a strong correlation between two parameters, it means that the spectrum changes in a similar way due to the change of the different parameters, making it difficult to separate their effects.

During the calculation, the upper 2×2 off-diagonal elements were taken into account. The spectral correlation matrix is shown in Table 2. A weak correlation can be observed between the FBA and the CW shift, as well as between the azimuthal angle deviation and the CW shift; therefore, their effects can indeed be isolated from each other. As it was seen on the elements of the MM, there is a stronger relationship between the FBA and the azimuthal angle error; however, if the lower off-diagonal elements are also taken into account, the correlation with the azimuthal error will be significantly reduced. This is because the asymmetric structure at
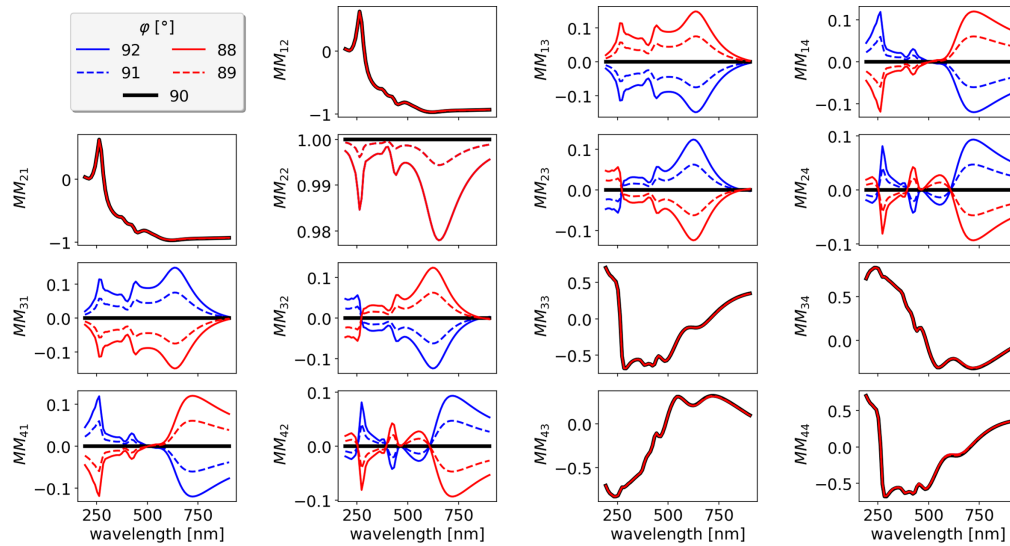
Fig. 6 MM for different azimuthal angle values. The importance of the exact alignment of the sample can be clearly observed. Even 1 deg error can produce comparable off-diagonal response to the asymmetries presented above.

Table 2 Spectral correlation matrix for the upper off-diagonal elements. The correlation coefficients show that the effects of the parameters can be distinguished from each other.

Parameters	FBA	CW shift	φ error
FBA	1	—	—
CW shift	−0.261	1	—
φ error	0.785	0.263	1

$\varphi = 90$ deg (Figs. 4 and 5) and the symmetric structure at $\varphi \neq 90$ deg (Fig. 6) elicit upper and lower off-diagonal responses with opposite signs, e.g., while in the former case $MM_{13} = MM_{31}$, in the latter case $MM_{13} = -MM_{31}$. The correlation between the FBA and the CW shift remains the same because the MM symmetries are the same for these parameters.

4.3 Investigating Correlations Between the Asymmetry and the Critical Dimension Parameters

If there is no asymmetry present in the structure, the off-diagonal elements will be zero at 90 deg azimuthal angle regardless of the critical dimension (CD) parameters, as it was described in Sec. 3. In this case, theoretically the correlation between CD and asymmetry parameters becomes exactly 0 for off-diagonal MM elements. However, if the structure is asymmetric, changes in the CD parameters can affect the off-diagonal response to asymmetry. To study the effect of crosstalk between CD and asymmetry parameters, a spectral correlation matrix was calculated for both the 8 off-diagonal elements and the whole MM (MM_{full}). In Table 3, a part of the correlation matrix is shown, focusing on asymmetry parameters. In the calculation, the nominal structure was asymmetric with the following asymmetry parameters: FBA = 1 deg, CW = 1 nm, φ error = 1 deg. The CD parameter names are shown in Fig. 7.

The correlation coefficients between FBA and CW shift are slightly different in Table 3 and Table 2, because the nominal parameters of the structure are not exactly the same (in case of Table 3, the nominal structure is asymmetrical, in Table 2 it is not). It can be observed that the correlation of FBA and CW shift with φ error indeed nearly disappears when calculated for all off-diagonal elements.

Table 3 Spectral correlation matrix, calculated for both MM_{off} and MM_{full}. It focuses on the relations between the asymmetry and CD parameters, showing a weak/moderated correlation between them.

Parameters	FBA		CW shift		φ error	
	MM_{off}	MM_{full}	MM_{off}	MM_{full}	MM_{off}	MM_{full}
FBA	1	1	—	—	—	—
CW shift	−0.263	−0.262	1	1	—	—
φ error	0.007	0.005	0.003	0.001	1	1
Pitch	−0.102	0.010	−0.264	0.019	−0.418	−0.070
CW CD	0.090	−0.006	0.079	−0.046	0.588	0.082
CW H	−0.277	−0.038	−0.113	−0.056	−0.295	−0.026
NS CD	0.102	−0.010	0.334	−0.002	0.422	0.076
Si H	0.037	0.017	0.153	0.048	0.284	−0.004
SiGe H	−0.045	0.001	0.008	0.064	0.121	−0.013
Wall H	−0.164	−0.040	0.201	0.002	−0.437	−0.037
STI H	0.013	0.006	0.185	0.050	0.286	0.045
Wall BH	0.194	0.036	0.141	0.077	0.501	0.016
STI SWA	−0.220	−0.049	−0.019	−0.025	−0.397	−0.057
SiO_2 liner	0.053	0.035	−0.170	−0.023	−0.149	−0.034
Si_3N_4 liner	0.204	0.037	0.022	0.033	0.486	0.078
Offset	−0.127	−0.037	0.066	0.019	−0.307	−0.025
β	−0.191	−0.035	0.005	−0.019	−0.367	−0.007
α	0.138	−0.005	−0.510	−0.061	−0.222	0.007
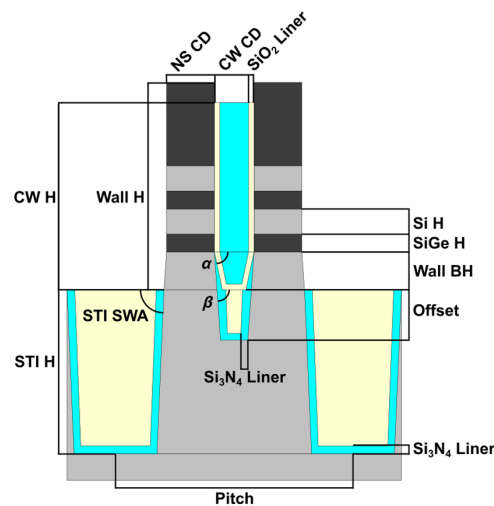
Fig. 7 Illustration and naming of CD parameters used in the correlation studies. The studied asymmetry parameters are illustrated in Fig. 3.

In each case, the spectral correlation matrix was calculated that contains the correlation coefficients when only two parameters are floated at a time, thus eliminating the influence of other parameters.[25] Table 3 shows that even if only the off-diagonal elements are considered, there will not be a strong correlation between asymmetry and CD parameters, with the highest value below $|0.6|$. However, when the whole MM is considered, the values of the correlation coefficients drop below $|0.1|$. The parameter correlation matrix[25] was also calculated (not shown here), when all parameters are floated at a time; therefore, the combined effect of all parameters appears in it. The correlations are not significant in this case either, the highest value being $|0.6|$ for MM_{off} and $|0.3|$ for MM_{full}.

To further study the measurement sensitivity, in Fig. 8, the RMSE between the MM for the nominal structure mentioned above and the MM obtained for a given parameter change (1 nm or 1 deg in all cases) is shown, for both MM_{off} and the rest of the MM elements (MM_{12}, MM_{21}, MM_{33}, MM_{34}, MM_{43}, and MM_{44}), respectively.

The sensitivity analysis (Fig. 8) shows that the off-diagonal elements of the MM around azimuth 90 deg are sensitive to structural asymmetries while they have reduced sensitivity to all other CD parameters [Fig. 8(a)]. The opposite holds for the other MM elements [Fig. 8(b)]. In addition to the low correlation coefficient values, this also increases confidence in the evaluation of asymmetry parameters from measurements performed in this configuration, even in the presence of small uncertainties in other CD parameters. Similar results were previously reported and experimentally confirmed in case of simpler structures for overlay and tilt metrologies.[21,24]

The combination of the parameter correlation matrix (Table 3) and sensitivity analysis (Fig. 8) clearly shows that the effects of changes in asymmetry and in CD parameters can be distinguished by MM-SE measurement.

It can be noticed how dominant the effect of the azimuthal angle error is compared to the other asymmetry parameters. The correlation between them is low for all MM off-diagonal elements; however, it has such a strong effect that a clearer picture of presence of asymmetry can be obtained by eliminating it. This can be particularly useful if one wants to detect asymmetry without modeling.[21] In the following section, a possible method for filtering out the azimuthal error will be presented.
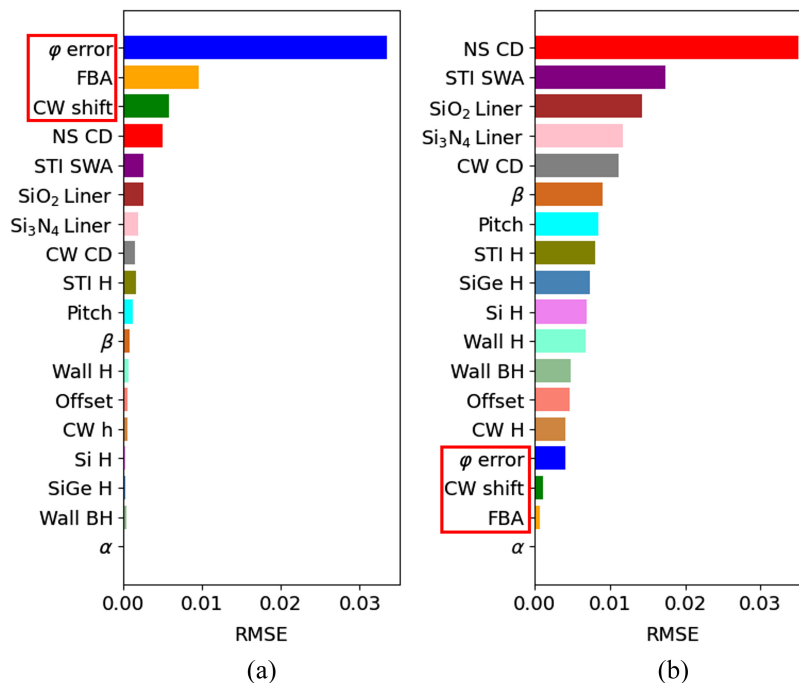
Fig. 8 Parameter sensitivity analysis. RMSE between the MM for the nominal structure and the MM obtained for a given parameter change (1 nm or 1 deg) for (a) MM_{off} and (b) MM_{12}, MM_{21}, MM_{33}, MM_{34}, MM_{43}, MM_{44} elements. The asymmetry parameters are framed in the figure.

$$RMSE = \sqrt{\frac{\sum_i (MM^{90°}_{off, i} - MM^{diff}_{off, i}/2)^2}{number\ of\ data\ points}}$$
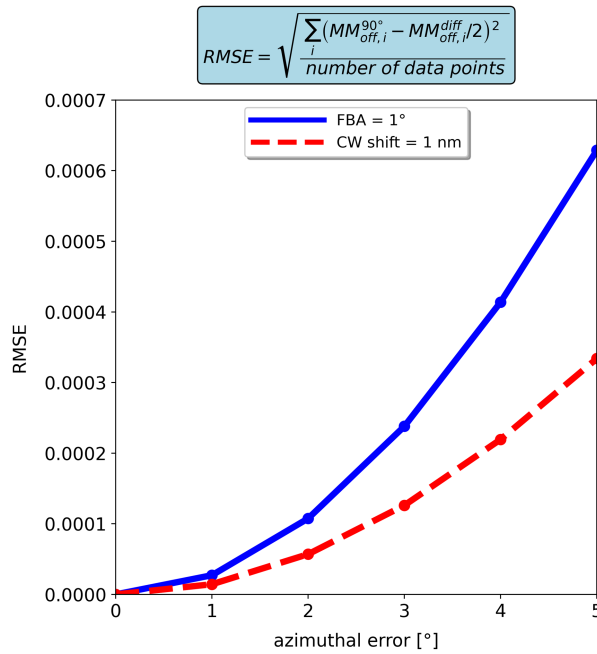
Fig. 9 RMSE between the MM off-diagonal elements obtained in the case of 90 deg azimuthal angle and elements calculated from $MM_{diff} = (MM^{90°-error}_{off} - MM^{-90°-error}_{off})/2$ with increasing azimuthal error, showing the validity of approximation in Eq. (7). In the two plotted cases, the elements do not differ significantly even in the case of 5 deg azimuthal angle error. With this method, the response caused by the azimuthal uncertainty can be filtered out of the off-diagonal elements.

4.4 Detection and Elimination of the Alignment Error by 180 deg Rotation of the Grid

Simulations were run to investigate the validity of Eq. (7) to filter out the azimuthal alignment error around $\varphi = 90.0$ deg.

With increasing azimuthal error, the discrepancy was investigated between half of the difference MM_{off} $((MM^{90°-error}_{off} - MM^{-90°-error}_{off})/2)$ and the MM_{off} obtained at 90 deg azimuthal angle in the presence of 1 deg FBA or 1 nm CW shift (Fig. 9). The simulations show that even with a 5 deg azimuthal angle deviation, they do not significantly differ. As an example, a visual comparison of the two MMs in the case of 1 deg FBA is shown in Fig. 10.
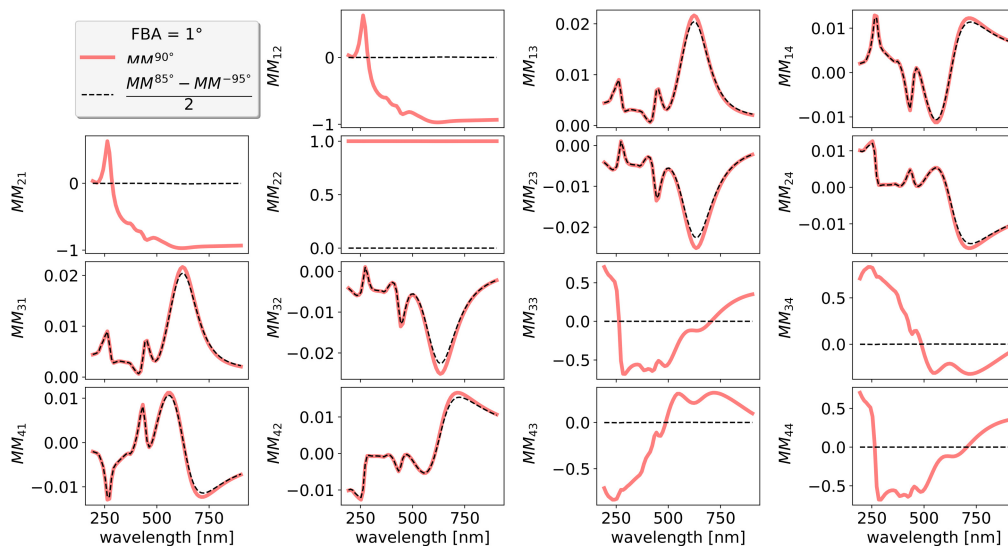
Fig. 10 Comparison of $MM^{90°}$ and $(MM^{85°} - MM^{-95°})/2$ in the presence of 1 deg FBA. A good agreement can be observed between the two MM spectra.

As a consequence, if the sample cannot be aligned precisely at 90 deg azimuthal angle, but a stage is available that enables accurate sample rotation, the effect of the azimuthal error can be eliminated, and the optical response resulting from the asymmetry can appear.

5 Conclusion

We have presented the relevant symmetry properties of MM elements which are important to consider in order to detect structural symmetry breaking of the measured samples. These symmetry relations provide a way to distinguish between sources of MM off-diagonal responses, allowing the separation of measurement inaccuracy from structural defects.

In the case of forksheet FET, we investigated the effect of different structural asymmetries on the MM with the help of simulations using RCWA method. We calculated MM spectra with different magnitudes and directions of defects at 90 deg azimuthal angle. The link between the asymmetry parameters was investigated by calculating the correlation coefficients.

The off-diagonal elements of the MM are sensitive to both the defect's magnitude and direction. The optical responses caused by the different non-uniformities can be separated from each other, making it possible to identify them by MM measurements. Our results also show the necessary measurement precision required to characterize these structural imperfections. It has been presented that the change in the asymmetry and CD parameters can be distinguished from each other, especially if the whole MM is taken into account in the evaluation.

Since uncertainty may arise in the exact aligning of the sample in azimuthal direction during the real measurement, the effect of its resulting error was also investigated. This, like asymmetries, also leads to an off-diagonal response; however, with due care it is possible to separate the two effects. A method was presented to filter out the effect of such alignment errors, assuming an accurate sample rotation stage is available.

References

1. P. Weckx et al., "Novel forksheet device architecture as ultimate logic scaling device towards 2 nm," in *IEEE Int. Electron Devices Meet. (IEDM)*, San Francisco, California, pp. 36.5.1–36.5.4 (2019).
2. D. Dixit et al., "Characterization of overlay and tilt in advanced technology nodes using scatterometry," in *30th Annu. SEMI Adv. Semicond. Manuf. Conf. (ASMC)*, Saratoga Springs, NY, USA, pp. 1–7 (2019).
3. C. Li, H. Zhao, and G. Mao, "Fin bending mechanism investigation for 14 nm FinFET technology," in *China Semicond. Technol. Int. Conf. (CSTIC)*, Shanghai, pp. 1–3 (2017).
4. A. Heinrich et al., "Photomask CD and LER characterization using Mueller matrix spectroscopic ellipsometry," *Proc. SPIE* **9231**, 92310L (2014).
5. D. Dixit et al., "Nonconventional applications of Mueller matrix-based scatterometry for advanced technology nodes," *J. Micro/Nanolithogr. MEMS MOEMS* **17**(3), 034001 (2018).
6. J. N. Hilfiker, N. Hong, and S. Schoeche, "Mueller matrix spectroscopic ellipsometry," *Adv. Opt. Technol.* **11**(3–4), 59–91 (2022).

7. J. Bogdanowicz et al., "Model-free measurement of lateral recess in gate-all-around transistors with micro hard-X-ray fluorescence," *J. Micro/Nanopattern. Mater. Metrol.* **22**(3), 034001 (2023).

8. R. Ciesielski et al., "Pushing the boundaries of EUV scatterometry: reconstruction of complex nanostructures for next-generation transistor technology," *Proc. SPIE* **12496**, 124961M (2023).

9. M. G. Moharam and T. K. Gaylord, "Rigorous coupled-wave analysis of planar-grating diffraction," *J. Opt. Soc. Am.* **71**(7), 811–818 (1981).

10. M. G. Moharam et al., "Formulation for stable and efficient implementation of the rigorous coupled-wave analysis of binary gratings," *J. Opt. Soc. Am.* **12**(5), 1068–1076 (1995).

11. M. Neviére and E. Popov, *Light Propagation in Periodic Media*, Taylor & Francis Group, Boca Raton, Florida (2003).

12. M. G. Moharam et al., "Stable implementation of the rigorous coupled-wave analysis for surface-relief gratings: enhanced transmittance matrix approach," *J. Opt. Soc. Am.* **12**(5), 1077–1086 (1995).

13. J. J. Hench, Z. E. Strakoš, and S. Strakoš, "The RCWA method: a case study with open questions and perspectives of algebraic computations," *Electron. Trans. Numer. Anal.* **31**, 331–357 (2008).

14. H. Fujiwara, *Spectroscopic Ellipsometry*, Maruzen Co. Ltd., Tokyo (2007).

15. L. Li, "Symmetries of cross-polarization diffraction coefficients of gratings," *J. Opt. Soc. Am. A* **17**(5), 881–887 (2000).

16. M. Korde et al., "Nondestructive characterization of nanoscale subsurface features fabricated by selective etching of multilayered nanowire test structures using Mueller matrix spectroscopic ellipsometry based scatterometry," *J. Vac. Sci. Technol. B* **38**(2), 024007 (2020).

17. R. J. Potton, "Reciprocity in optics," *Rep. Progr. Phys.* **67**, 717–754 (2004).

18. Y.-N. Kim et al., "Device based in-chip critical dimension and overlay metrology," *Opt. Express* **17**(23), 21336–21343 (2009).

19. T. Novikova et al., "Metrological applications of Mueller polarimetry in conical diffraction for overlay characterization in microelectronics," *EPJ Appl. Phys.* **31**, 63–69 (2005).

20. X. Chen et al., "Towards understanding the detection of profile asymmetry from Mueller matrix differential decomposition," *J. Appl. Phys.* **118**(22), 225308 (2015).

21. J. Li et al., "Mueller matrix measurement of asymmetric gratings," *J. Micro/Nanolithogr. MEMS MOEMS* **9**(4), 041305 (2010).

22. T. Novikova et al., "Mueller polarimetry as a tool for detecting asymmetry in diffraction grating profiles," *J. Vac. Sci. Technol. B* **29**(5), 051804 (2011).

23. T. Novikova and P. Bulkin, "Inverse problem of Mueller polarimetry for metrological applications," *J. Inverse Ill-Posed Probl.* **29**, 759–774 (2021).

24. J. Li et al., "Advanced diffraction-based overlay for double patterning," *Proc. SPIE* **7638**, 76382C (2010).

25. P. Vagos et al., "Uncertainty and sensitivity analysis and its applications in OCD measurements," *Proc. SPIE* **7272**, 72721N (2009).

Boglárka Dikó received her BSc and MSc degrees in chemical engineering from Budapest University of Technology and Economics in 2017 and 2019, respectively. She is currently an application scientist at Semilab Ltd., Ellipsometry Department, OCD team.

Roberta Zsófia Kiss received her BSc and MSc degrees in physics from Budapest University of Technology and Economics in 2020 and 2022, respectively. Her thesis focused on non-Hermitian quantum dynamics. Currently, she is an application scientist at Semilab Ltd., Ellipsometry Department, OCD team.

Dávid Egri received his MSc degree in physics from Budapest University of Technology and Economics in 2020. His thesis focused on developing sensitivity and uncertainty analysis for optical critical dimension (OCD) metrology while working as application scientist trainee at Semilab Co. Ltd. After graduation, he joined the company full time where he is currently a scientific software developer and software product owner working on a measurement evaluation software solution for OCD metrology.

Emeric Balogh is a senior application scientist at Semilab, Ellipsometry Department. His focus is the development of model-based dimension metrologies, ellipsometry, and scatterometry. He received his BSc degree in physics and computer science and his MSc degree in computational physics from Babes-Bolyai University. He received his PhD from the University of Szeged, with a thesis in attosecond physics and metrology.